

Edge function analysis of stress intensity factors in cracked anisotropic plates

J.F. DWYER and E. PAN

Department of Civil Engineering, University of Colorado, Boulder, CO 80309, U.S.A.

Received 21 August 1994; accepted in revised form 10 April 1995

Abstract. The edge function method, which involves the use of analytic solutions to model field behavior in the various parts of an elastic region, is applied to the analysis of a finite anisotropic plate with a single crack. Analytical solutions for the stress singularities at each crack tip facilitate the inexpensive calculation of accurate values of the stress intensity factors. A boundary Galerkin variational principle is used to match the boundary conditions. The method is applicable to isotropic and anisotropic materials and is demonstrated for a number of fracture problems involving variation of the crack position, crack orientation and material orientation. For the range of geometries examined in this paper, the calculated values of the stress intensity factors do not show a major dependence on the material anisotropy. The formulation of the method makes it easily applicable to the study of the interaction of several cracks and also to a limited study of crack propagation or damage development in a composite laminate.

1. Introduction

Applications of composite materials continue to increase and the associated fracture problems occupy the attention of many researchers. In some cases the composite may be modeled as a finite anisotropic plate while in other cases such a plate can be considered as a basic building block for a laminated structure. In either instance the analysis of such plates provides a valuable insight into the behavior of composite structures. Such an analysis is required to supplement the work already performed for isotropic plates and also to examine the effects of a finite boundary compared to the well documented results for the infinite case.

This paper describes the use of the edge function technique to study the stress intensity factors of a crack in a finite anisotropic plate. The edge function method involves the use of analytical solutions to model the field behavior in various parts of the domain under investigation. The essence of the edge function approach is the approximation of the solution of a boundary-value problem by a linear combination of solutions of the field equations. A set of solutions is generated which can model arbitrary effects on each boundary (edge functions) and which exhibit rapid decay away from that boundary. Singular solutions corresponding to vertices, cracks, holes and concentrated loads are also included to provide a rapidly convergent analytical solution. The edge functions and singular solutions are based on the complex variable formulation. The unknowns in the linear combination are obtained from a system of equations which follows from the approximation of the boundary conditions by a boundary Galerkin energy method.

Dwyer [1] gives a review of edge function work and presents accurate solutions for a range of singular problems. These include problems with mixed boundary conditions, singular loads and elliptical cutouts as well as arbitrarily oriented cracks. The method is particularly well suited to solving crack problems since an analytical approach is used to model the singularities, which requires much less computational time than the conventional numerical methods such

as finite elements or boundary elements. The accuracy of the results in the edge function analysis makes it an appropriate tool for an extensive parametric study of crack behavior as crack angle, crack position and fibre orientation are modified. Furthermore, it is possible to combine the edge function method with other standard methods such as finite elements, wherein the singularity is modeled by edge functions and far-field behavior is modeled by finite elements. The model can also handle isotropic data as a special case simply by perturbing the material constants by a very small amount and the solution has been shown to be highly stable for such perturbations.

The next section provides a brief review of existing work. That is followed by a summary of the complex variable formulation of anisotropic elasticity and a description of the edge function representation of the solutions of the associated boundary value problems. The boundary-Galerkin method is then described, followed by the formulae for stress intensity factors. Numerical results are then presented in order to illustrate the accuracy and efficiency of this new method and also in order to examine the influence of crack orientation, material orientation and proximity of the boundary on the stress intensity factors. The final section presents some conclusions and discusses possible extensions of the current work.

2. Review

Much of the work performed on the fracture of anisotropic plates has utilized the finite element method. The method has been augmented in many ways to include a special element to deal with the crack singularity. Pian et al. [2] developed a hybrid finite element formulation and Mandell et al. [3] used this technique in studying stress intensity factors in anisotropic single edge notched, double edge notched and double cantilever beam fracture toughness specimens. Foschi and Barrett [4] used conforming isoparametric elements and a singular displacement field around the crack in an anisotropic plate. Tong [5] used a hybrid finite element approach to solve crack problems in a plate with rectilinear anisotropy. Soni and Stern [6] used a reciprocal work contour integral method to calculate the intensity of singular stress states at cracks in orthotropic plates but used the finite element method to model the field behavior, while Atluri et al. [7] obtained stress intensity correction factors for angle-ply laminates using the finite element method.

The boundary integral equation method has also been widely used. Snyder and Cruse [8] obtained numerical results for center-cracked and double-edge cracked finite width tension specimens using material properties representative of a family of advanced fiber reinforced composite laminates. Karami and Fenner [9] and Blandford et al. [10] also used the boundary integral equation method, while Cruse and Wilson [11] combined the latter method with the finite element method.

In addition to the above, some other numerical techniques have also been applied. Bowie and Freese [12] calculated the stress intensity factors for the plane problem of a central crack in a rectangular sheet of orthotropic material using an extension of the modified mapping collocation method [13]. Gandhi [14] investigated the problem of an inclined crack in an orthotropic rectangular plate under tension, using a modified mapping collocation method. A recent paper by Yum and Hong [15] uses the same method for the mixed mode fracture problem, where an inclined crack parallel to the fiber direction is considered. They present stress intensity correction factors for a range of crack lengths, crack angles, material properties and plate aspect ratios. A similar study is provided by Gyekenyesi and Mendelson [16] for a rectangular orthotropic center-cracked plate. They also used a mapping collocation technique.

Satapathy and Parhi [17] determined stress and displacement fields for the case of a crack situated symmetrically and oriented normal to the edges of an orthotropic elastic strip by using a reduction to Fredholm integral equations.

Some very recent publications show that there continues to be much interest in the cracked anisotropic plate. Chen and Atluri [18] present a general two-dimensional finite element alternating method for the determination of weight functions for isotropic or orthotropic cracked structures subjected to mixed mode loading. Woo and Wang [19] use the boundary collocation method to compute stress intensity factors for an internal crack in a finite anisotropic plate while Chen and Kudva [20] obtain stress intensity factors using a complex variable formulation in conjunction with a hybrid displacement finite element scheme.

3. Complex potential formulation of generalized plain strain

This section summarizes the formulation of the complex variable approach to anisotropic elasticity due to Lekhnitskii [21] and is included here for completeness. The modern subscript notation and the implied summation convention are adopted. In this paper, tensile normal stresses are taken to be positive.

Consider a cylindrical linearly anisotropic body which is deformed by body forces and surface tractions which act in a plane normal to the generators but do not vary along the generators. The deformation of the body is described in an (x_1, x_2, x_3) Cartesian coordinate system where the x_3 -axis is parallel to the generators. The body is assumed to deform under a condition of *generalized plane strain* in the (x_1, x_2) plane. In the (x_1, x_2, x_3) coordinate system, the components of displacement and strain are

$$u_i = u_i(x_1, x_2) \quad (1)$$

and

$$\varepsilon_{ij} = \frac{(u_{i,j} + u_{j,i})}{2}, \quad (2)$$

respectively (with $i, j = 1-3$). The constitutive model for the anisotropic medium is described by Hooke's law which can be written in matrix form as follows

$$\underline{\sigma} = \underline{C} \underline{\varepsilon} \quad (3)$$

or

$$\underline{\varepsilon} = \underline{A} \underline{\sigma}, \quad (4)$$

where

$$\underline{\varepsilon} = (\varepsilon_{11}, \varepsilon_{22}, \varepsilon_{33}, 2\varepsilon_{23}, 2\varepsilon_{13}, 2\varepsilon_{12})^T$$

are the strain components and

$$\underline{\sigma} = (\sigma_{11}, \sigma_{22}, \sigma_{33}, \sigma_{23}, \sigma_{13}, \sigma_{12})^T$$

are the stress components. \underline{A} is a (6×6) symmetric compliance matrix with 21 independent components $a_{ij}(i, j = 1, 6)$ and \underline{C} is the corresponding matrix of elastic parameters with

components c_{ij} ($i, j = 1, 6$) and is such that $C = A^{-1}$. The stresses must satisfy the equilibrium equations given by

$$\sigma_{ij,j} + f_i = 0, \quad (5)$$

where f_i ($i = 1-3$) are the components of the body force vector \underline{f} . In general, a particular integral can be developed to model the body force. The boundary conditions can then be modified to yield a boundary value problem with zero body forces [1]. In this case, it follows from Lekhnitskii [21] that the stresses and displacements have the following complex potential representations

$$\sigma_{ij} = \text{Re} \sum_{k=1}^3 s_{ijk} \Phi'_k(z_k) \quad (6)$$

and

$$u_i = \text{Re} \sum_{k=1}^3 p_{ik} \Phi_k(z_k), \quad (7)$$

where Re denotes the real part of a complex function and $\Phi'_k(z_k)$ ($k = 1, 2, 3$) denote the derivatives of three analytical stress functions $\Phi_k(z_k)$ of the variable $z_k = x_1 + \mu_k x_2$ where x_1 and x_2 are the coordinates of the point in the anisotropic medium at which the stresses and displacements are calculated. The parameters μ_k ($k = 1, 2, 3$) are complex numbers with positive imaginary parts and are the roots of a characteristic equation of the form [21]

$$\sum_{i=1}^6 c_i \mu^i = 0. \quad (8)$$

The coefficients, s_{ijk} , p_{ik} and c_i , in (6), (7) and (8) respectively, are functions of the compliance components a_{ij} ($i, j = 1-6$). If the body has a plane of symmetry normal to the generators (x_3 -axis), it can be shown that the body deforms in a *plane strain* manner and that the displacement and stress components depend on $\Phi_1(z_1)$ and $\Phi_2(z_2)$ only.

Representations (6) and (7) are sufficient also for the case when two or three of the roots of (8) coincide e.g. isotropic materials. It was found that formulae (6) and (7) are highly stable in the neighborhood of such materials and that there is no need to deal with such cases separately. Numerical solutions to such problems can be obtained by perturbing the elasticities slightly as shown by Grannell and Quinlan [22].

4. Potential function representation

Finite polygonal regions deforming in *plane strain*, such as the one shown in Fig. 1, are considered. The regions may contain cracks and circular or elliptical holes. In the edge function method, for a given polygonal region, the functions $\Phi_k(z_k)$ ($k = 1, 2$) appearing in (6) and (7) are expressed as follows

$$\Phi_k(z_k) = \sum_{n=1}^N \sum_{m=1}^{M_n} A_{kn}^m \phi_{kn}^m(z_k), \quad (9)$$

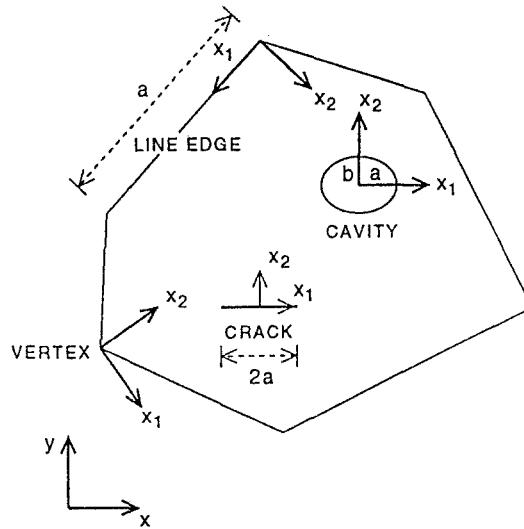


Fig. 1. A finite polygonal region with an internal crack and cavity.

where $\phi_{kn}^m(z_k)$ are analytic functions which satisfy the homogeneous form of the equilibrium equations (5) and A_{kn}^m are arbitrary constants which must be chosen to satisfy the boundary conditions of the region as well as possible. The rationale of the method is to choose functions $\phi_{kn}^m(z_k)$ which are capable of representing the solution in the neighborhood of critical parts of the region boundary such as straight line segments, angular corners (vertices), cracks and interior cavities. In (9), N is the number of such critical parts and M_n is the number of potential functions associated with critical part n . In general, the solution for each critical part is an infinite series truncated at M_n terms.

The notation (x_1, x_2) is used, in this section, to denote a local set of axes attached to each critical part $n = 1, N$ relative to which the potentials $\phi_{kn}^m(z_k)$ are defined. The notation $\mu_k(k = 1, 2)$ denotes the roots of (8) relative to the local set of axes. The equations of anisotropic elasticity are form-invariant under rotation of axes. The formula relating the roots of (8) to those relative to a rotated system of axes is given in Lekhnitskii [21].

4.1. EDGE AND VERTEX FUNCTIONS

In this section, particular forms of the potentials $\phi_{kn}^m(z_k)$ associated with each critical part of the boundary of the region of interest are described. These forms are used to model arbitrary displacements or tractions on each straight line edge or cavity edge of the region and are termed *edge functions*. System matrix stability considerations require that each edge function displacement and traction field decays away from the boundary with which it is associated. Singular solutions which satisfy homogeneous boundary conditions in the neighborhood of a vertex are included in the representation of the approximate solution in order to accelerate convergence. Such solutions are termed *vertex functions*.

4.1.1. Line edge functions

Consider the finite polygonal region of Fig. 1. Let (x_1, x_2) be a local coordinate system attached to one of its line edges of length a . The x_1 -axis is directed along the edge and the

x_2 -axis points into the interior of the region. The origin of the local coordinate system is at one end of the edge. For edge number n the edge function complex potentials are [1]

$$\phi_{kn}^m(z_k) = e^{imz_k}; \quad k = 1, 2, \quad (10)$$

where

$$m = \frac{2\pi M}{a}; \quad M = 1, 2, \dots, M_n.$$

The displacements and stresses computed by combining (6), (7), (9) and (10) decay exponentially away from the edge into the interior, are periodic in x_1 with period a , and reduce to trigonometric polynomials on the edge. The higher edge function harmonics decay rapidly away from each edge and hence contribute to the stability of the system matrix.

The potentials (10) must be supplemented by potentials with two further degrees of freedom in order to model arbitrary (aperiodic) effects on each edge. In particular, the auxiliary potentials must yield displacements/tractions which are non-zero at $x_1 = 0$ and $x_1 = a$. One choice for such auxiliary potentials is given by [1]

$$\phi_{kn}^m(z_k) = z_k^m; \quad m = 1, 2, \dots, M_n; \quad k = 1, 2. \quad (11)$$

These functions are known as *polar functions* and are defined with respect to an origin at the center of the region.

4.1.2. Cavity and crack edge functions

Consider now elliptical cavity, n , in the polygonal region of Fig. 1 with major and minor semi-axes, a and b respectively. Let (x_1, x_2) be a local coordinate system attached to that cavity with origin at the center of the cavity. For the cavity of Fig. 1, the complex potentials are given by [21]

$$\phi_{kn}^m(z_k) = \xi_k^{-m}; \quad m = 1, 2, \dots, M_n; \quad k = 1, 2, \quad (12)$$

where

$$\xi_k = \frac{z_k + \sqrt{(z_k^2 - a^2 - \mu_k^2 b^2)}}{(a - i\mu_k b)}. \quad (13)$$

The potentials (12) are based on a conformal mapping of the exterior of the ellipse onto that of the unit circle. That branch of the square root in (13) is taken which ensures decay away from the elliptical edge. The tractions corresponding to (12) are self-equilibrated on the elliptical edge. The potentials (12) reduce to trigonometric polynomials in θ where $\theta = \arg(\xi_k)$ on the edge.

Crack edge functions can be obtained from the cavity edge functions simply by setting $b = 0$ in (13). The square root singularity at the crack tips may be seen by examining the derivatives of $\phi_{kn}^m(z_k)$ with respect to z_k , e.g.

$$\phi_{kn}^{m'} = \frac{-m\xi_k^{-m}}{\sqrt{(z_k^2 - a^2)}}; \quad m = 1, 2, \dots, M_n; \quad k = 1, 2. \quad (14)$$

4.1.3. Vertex functions

Consider now vertex, n , of the finite polygonal region in Fig. 1 and let (x_1, x_2) be a local coordinate system with origin at that vertex. Solutions of (5) which satisfy zero boundary conditions (displacement and/or traction) on each side of the vertex in Fig. 1 are sought in the form

$$\phi_{kn}(z_k) = E_{kn} z_k^{\lambda_n}; \quad k = 1, 2, \quad (15)$$

where E_{1n} and E_{2n} are complex constants. Imposition of the boundary conditions on each side of the vertex yields a 4×4 linear system of equations

$$A(\lambda_n) \underline{e} = 0, \quad (16)$$

where \underline{e} is the vector of real and imaginary parts of the constants E_{1n} and E_{2n} in (14). The existence of non-trivial solutions of (15) requires that

$$|A(\lambda_n)| = 0, \quad (17)$$

which yields the set $\{\lambda_n^1, \lambda_n^2, \dots, \lambda_n^M\}$ of exponents (both real and complex exponents occur). If $\text{Re}(\lambda_n) < 1$, then the stresses are singular, as can be seen by substituting (14) in (6).

5. The boundary Galerkin method

The representation of the approximate solution of the boundary value problem has the form given by (6) and (7) where, according to (9), the complex potentials, $\Phi_k(z_k)$, consist of linear combinations of edge functions, vertex functions and polar functions. Thus, the equilibrium equations (5) are satisfied *a-priori* if appropriate particular integrals are subtracted to yield a modified problem with zero body forces. The only remaining step is to determine the coefficients appearing in the edge, vertex and polar function potentials from the boundary conditions of the boundary value problem. This is done using the boundary Galerkin method.

The boundary Galerkin method is based on an abstract principle of virtual work, which is equivalent to the minimization of the strain energy error in the case of traction or displacement problems. The set of admissible displacements consists of the finite-strain-energy displacements which satisfy (5) with $\underline{f} = \underline{0}$ and from which rigid-body displacements are excluded. Let $\{\underline{h}_1, \underline{h}_2, \dots, \underline{h}_N\}$ be a basis for a finite dimensional sub-space of the above set and let $\underline{t}(\underline{h}_j)$ be the traction vector (computed from the displacement \underline{h}_j using (2) and (3) on the boundary). The boundary of the region is denoted by Γ . Traction is specified on Γ_t and displacements on Γ_u with $\Gamma = \Gamma_t + \Gamma_u$. The boundary conditions are

$$\underline{t}(\underline{u}) = \bar{\underline{t}} \quad \text{on} \quad \Gamma_t \quad (18a)$$

and

$$\underline{u} = \bar{\underline{u}} \quad \text{on} \quad \Gamma_u, \quad (18b)$$

where the boundary values of traction and displacement are indicated by overbars. As shown by Dwyer [1], the system equations have the form

$$G \underline{c} = \underline{b}, \quad (19)$$

where

$$G_{ij} = \int_{\Gamma_t} \underline{t}(\underline{h}_j) \cdot \underline{h}_i \, ds - \int_{\Gamma_u} \underline{t}(\underline{h}_i) \cdot \underline{h}_j \, ds \quad (20)$$

and

$$b_i = \int_{\Gamma_t} \bar{\underline{t}} \cdot \underline{h}_i \, ds - \int_{\Gamma_u} \underline{t}(\underline{h}_i) \cdot \bar{\underline{u}} \, ds. \quad (21)$$

In (19), \underline{c} is the vector of the unknown coefficients in the edge, vertex and polar function potentials. Matrix \mathbf{G} is symmetric and positive definite for displacement or traction problems.

Boundary values and errors of the approximate solution are computed at a number of equidistant points on each boundary. The errors are computed in terms of the differences (residuals) between the prescribed and computed quantities at each of these points. For convenience, the root mean square of the residuals is used as a concise measure of accuracy. Displacements and tractions on specified lines and curves are also computed as well as circumferential stresses on the surface of each cavity.

The coefficients A_{kn}^m ($k = 1, 2$) in (9) are, in general, complex constants. Hence each value of m on each critical part, n , has four real constants associated with it, giving rise to four degrees of freedom (or unknowns) in the system of equations (19). This is true for polar functions and line and cavity edge functions. In the case of homogeneous vertex functions, the number of degrees of freedom depends on the number of vertex functions chosen in the particular representation for each vertex. Particular solutions which are used to modify the boundary conditions do not contribute to the total number of degrees of freedom. The relationship between the potential functions and the degrees of freedom is described in greater detail in Dwyer and Amadei [23].

6. Calculation of stress intensity factors

It is assumed that the crack propagates in a self-similar manner. The stress intensity factors for mode I and mode II crack propagation are defined

$$\begin{aligned} K_I &= \lim_{x_1 \rightarrow a} \sqrt{2(x_1 - a)} \sigma_{22}|_{x_2=0}, \\ K_{II} &= \lim_{x_1 \rightarrow a} \sqrt{2(x_1 - a)} \sigma_{12}|_{x_2=0}, \end{aligned} \quad (22)$$

where (x_1, x_2) are Cartesian coordinates relative to a system of axes with center at the middle of the crack with the x_1 -axis directed along the crack. It follows from (6), (12), (13) and (22) that, for crack, n ,

$$\begin{aligned} K_I &= -\text{Re} \sum_{m=1}^{M_n} m(\alpha_{1m}^n + \alpha_{2m}^n)/\sqrt{a}, \\ k_{II} &= -\text{Re} \sum_{m=1}^{N_n} m(\mu_1 \alpha_{1m}^n + \mu_2 \alpha_{2m}^n)/\sqrt{a}, \end{aligned} \quad (23)$$

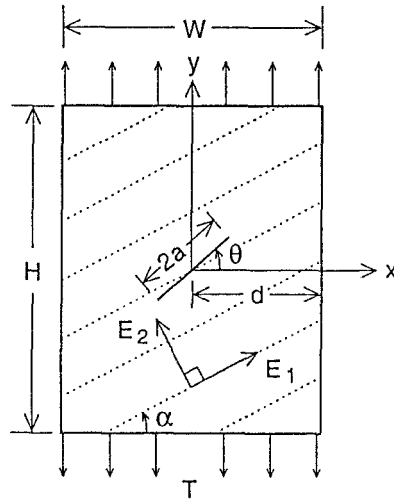


Fig. 2. A cracked anisotropic plate under uni-directional tension T .

where α_{km}^n are the particular A_{kn}^m in (9) which correspond to the cavity edge functions for crack, n . The above formulae apply to the crack tip at $x_1 = a$. Similar formulae apply to the tip at $x_1 = -a$.

7. Numerical examples

In the examples presented here the material parameters are defined in terms of Young's moduli, shear moduli and Poisson's ratios in a global (x, y, z) coordinate system such that the x and z -axes are horizontal and the y -axis is vertical upwards. The compliances a_{ij} of matrix A in (4) are such that

$$\begin{aligned} a_{11} &= \frac{1}{E_1}, & a_{22} &= \frac{1}{E_2}, & a_{33} &= \frac{1}{E_3}, \\ a_{12} &= -\frac{\nu_{21}}{E_2}, & a_{13} &= -\frac{\nu_{31}}{E_3}, & a_{23} &= -\frac{\nu_{32}}{E_3}, \\ a_{44} &= \frac{1}{G_{23}}, & a_{55} &= \frac{1}{G_{13}}, & a_{66} &= \frac{1}{G_{12}}, \end{aligned} \quad (24)$$

where E_1, E_2 and E_3 are Young's moduli in the 1, 2, 3 directions parallel to the x, y and z axes, respectively. The moduli G_{12}, G_{13} and G_{23} are, respectively, shear moduli in planes parallel to the xy, xz and yz planes. Finally, ν_{ij} ($i, j = 1, 2, 3$) are the Poisson's ratios that characterize the normal strains in the symmetry directions i when a stress is applied in the symmetry directions j . Because of symmetry of the compliance matrix A , Poisson's ratios ν_{ij} and ν_{ji} are such that $\nu_{ij}/E_i = \nu_{ji}/E_j$.

Because of the theory of linear elasticity, the stresses depend only on ratios of elastic constants and ratios of geometric dimensions. Therefore, the geometric units used in the following examples are immaterial. In all cases the stress intensity factors are normalized with respect to the applied load T and with respect to the square root of half crack length (Fig. 2).

The success of the edge function method for anisotropic fracture problems is well documented (Dwyer [1], Dwyer and Amadei [24]). These references illustrate the applicability of

Table 1. Stress intensity factors for crack in anisotropic plate

	K_I	K_{II}
Foschi and Barrett [4]	0.515	0.543
Gandhi [14]	0.519	0.514
Woo and Wang [19]	0.519	0.513
efm	0.519	0.513

the method for both traction and mixed boundary conditions. Extremely accurate solutions are obtained and stress intensity factors compare well with the literature. The first two examples here demonstrate such comparisons.

Example 1

This example is defined by the geometry in Fig. 2. In this first case $H = W = 10$ cm, $a = 1$ cm, $d = 5$ cm, θ (crack angle) = 45° and α (material angle) = 45° . The material constants are (in GPa) $E_1 = 48.265$, $E_2 = 17.238$, $G_{12} = 6.895$ and $\nu_{12} = 0.29$, which represent the smeared out properties of fiber-glass [14].

The problem was solved using just 51 degrees of freedom. All root mean square residuals were less than 1 percent of the applied load. This indicates that an extremely accurate solution has been obtained. Table 1 presents the current results (denoted 'efm') as well as those of several other researchers. The close agreement of the results is obvious.

Example 2

An example involving an isotropic material is included now to provide further comparison with the literature. In this case (refer to Fig. 2) $H = 8.484$ cm, $W = 2.828$ cm, $a = 1$ cm, $d = 1.414$ cm and $\theta = 45^\circ$. The edge function results and those of other researchers are presented in Table 2.

Convergence of the solution in this case required a higher number of degrees of freedom than in the previous example. However it has been found in previous edge function work that convergence is faster on the crack surface than on the exterior boundaries. It is clear from the final results that the computed stress intensity factors closely match those reported in the literature.

Example 3

The variation of the stress intensity factors with respect to the orientation of the crack is considered in this example. The plate and crack dimensions are identical to those of Example 1 and three types of material are examined. One material is isotropic. The second is Glass/Epoxy [15] with material properties (in GPa) defined by $E_1 = 48.27$, $E_2 = 17.24$, $G_{12} = 6.9$ and $\nu_{12} = 0.29$ and the third material is Graphite/Epoxy [15] with material properties (in GPa) defined by $E_1 = 133.8$, $E_2 = 9.58$, $G_{12} = 4.8$ and $\nu_{12} = 0.28$. The material orientation is 0° in each case.

The stress intensity factors are calculated for crack orientations varying from 0° to 90° and the resultant normalized mode I and mode II values are plotted in Figs. 3 and 4, respectively. The mode I factors are all at a maximum when the crack is perpendicular to the applied load and decrease smoothly to a minimum value of zero when the crack is parallel to the applied

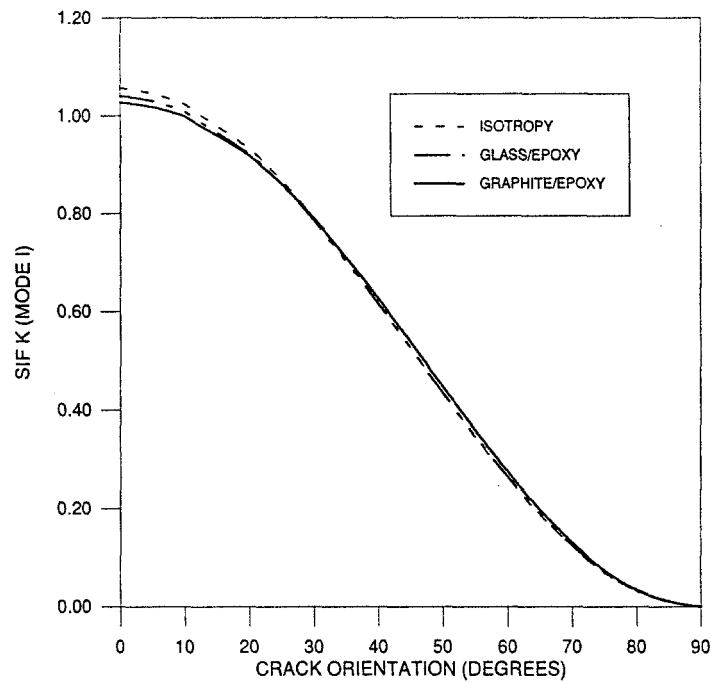


Fig. 3. Variation, with crack orientation, of the normalized stress intensity factors $K_I / (T\sqrt{a})$ for isotropic, glass/epoxy, and graphite/epoxy materials. The material angle $\alpha = 0^\circ$.

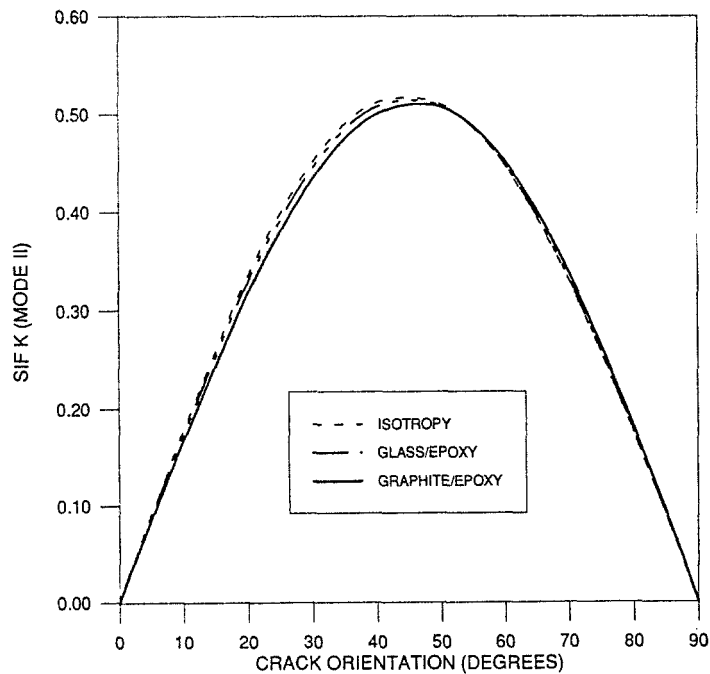


Fig. 4. Variation, with crack orientation, of the normalized stress intensity factors $K_{II} / (T\sqrt{a})$ for isotropic, glass/epoxy, and graphite/epoxy materials. The material angle $\alpha = 0^\circ$.

Table 2. Stress intensity factors for crack in isotropic plate

	K_I	K_{II}
Cruse and Wilson [11]	0.728	0.590
Karami and Fenner [9]	0.732	0.591
Blandford et al. [10]	0.725	0.598
Yum and Hong [15]	0.727	0.591
efm (67 degrees of freedom)	0.715	0.572
efm (99 degrees of freedom)	0.725	0.588

load. The mode II factors are zero when the crack is perpendicular to the load and reach a maximum when the crack is oriented at 45° . They then decrease to zero again when the crack is parallel to the load. A comparison of Figs. 3 and 4 shows that both modes I and mode II stress intensity factors are equal when the crack is oriented at 45° to the applied load. This is of course the situation where both modes of fracture propagation are expected to be the same. It is also interesting to note that the effects of the anisotropy are almost negligible in this example. A convergence study of one of the cases here, involving the more anisotropic Graphite/Epoxy material, showed that both the mode I and mode II stress intensity factors stabilized to three decimal places when 71 degrees of freedom were used.

Example 4

This case concerns the calculation of stress intensity factors when the orientation of the material is varied. The plate and crack geometry are the same as in the previous example except that here the crack orientation is fixed at an angle of 45° to the applied load. The same materials (Glass/Epoxy, Graphite/Epoxy and isotropic) as in the previous example are used.

The material orientation is varied from 0° to 90° and the resultant mode I and mode II stress intensity factors are plotted in Figs. 5 and 6, respectively. The isotropic results provide a set of reference values. Both mode I and mode II factors for the anisotropic materials attain a minimum when the material is aligned at 45° to the horizontal (material axes are parallel to the crack) and a maximum when the material is aligned at 90° . The effects of the anisotropy can be seen in these results with greater variation being exhibited for the more strongly anisotropic Graphite/Epoxy material.

Example 5

In this final example the effects of the proximity of the boundary are considered by varying the position of the crack. The same geometric dimensions are used as in Example 1 and the material orientation and crack orientation are both kept at 0° to the horizontal. The Glass/Epoxy material defined above is used in this example as well as the case of the isotropic material.

The position of the crack is moved from the center of the plate to a position where the crack tip is only a distance of 1.5 times the crack length from the right-hand edge of the plate. The variations of the stress intensity factors at the right most crack tip and left most crack tip are plotted in Figs. 7 and 8 for the isotropic material and the Glass/Epoxy material respectively. There is an obvious increase in the values as the crack tip approaches the boundary. The effect is slightly more pronounced in the case of the isotropic material.

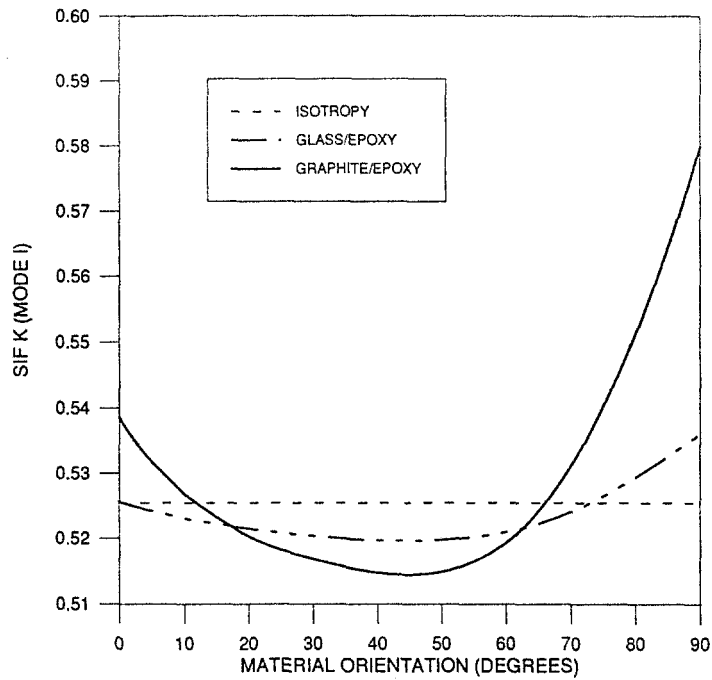


Fig. 5. Variation, with material orientation, of the normalized stress intensity factors $K_I/(T\sqrt{a})$ for isotropic, glass/epoxy, and graphite/epoxy materials. The crack angle $\theta = 45^\circ$.

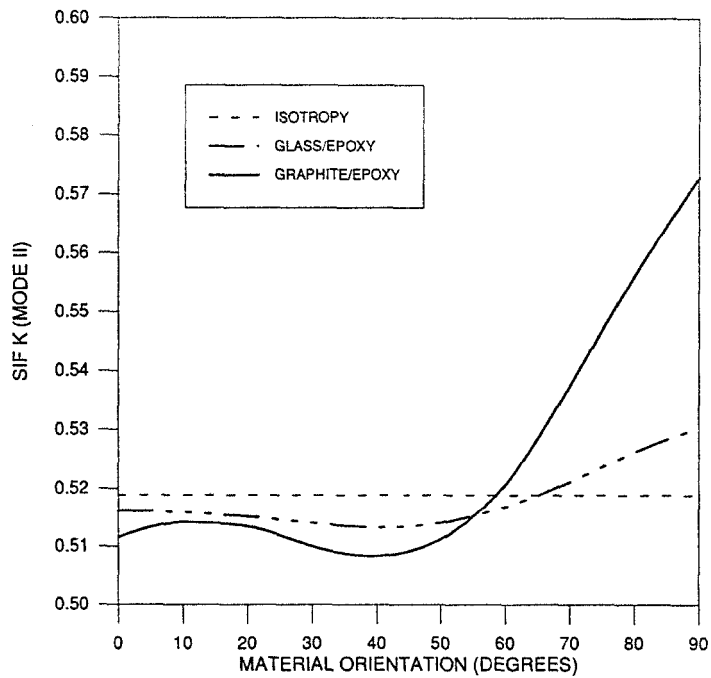


Fig. 6. Variation, with material orientation, of the normalized stress intensity factors $K_{II}/(T\sqrt{a})$ for isotropic, glass/epoxy, and graphite/epoxy materials. The crack angle $\theta = 45^\circ$.

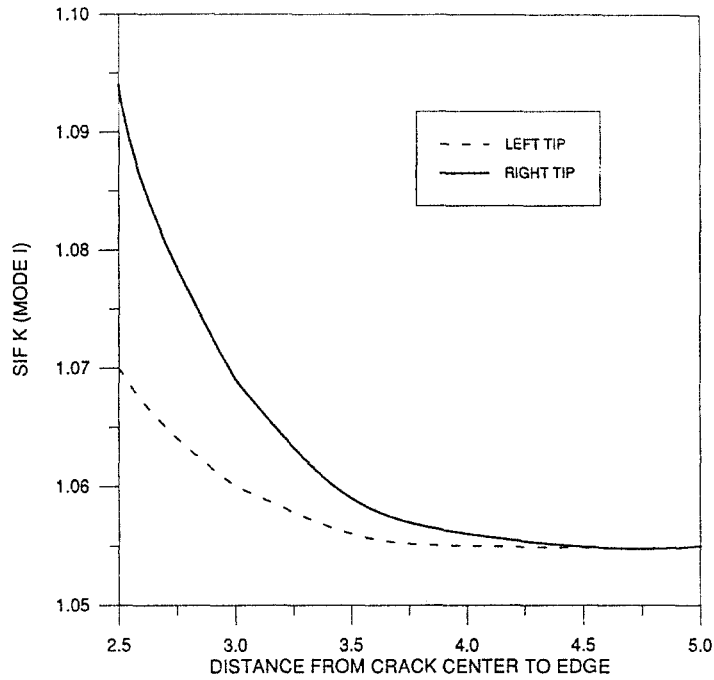


Fig. 7. Variation, with distance to the plate edge, of the normalized stress intensity factors $K_I/(T\sqrt{a})$ at left and right crack tips for the isotropic material. The crack angle $\theta = 0^\circ$.

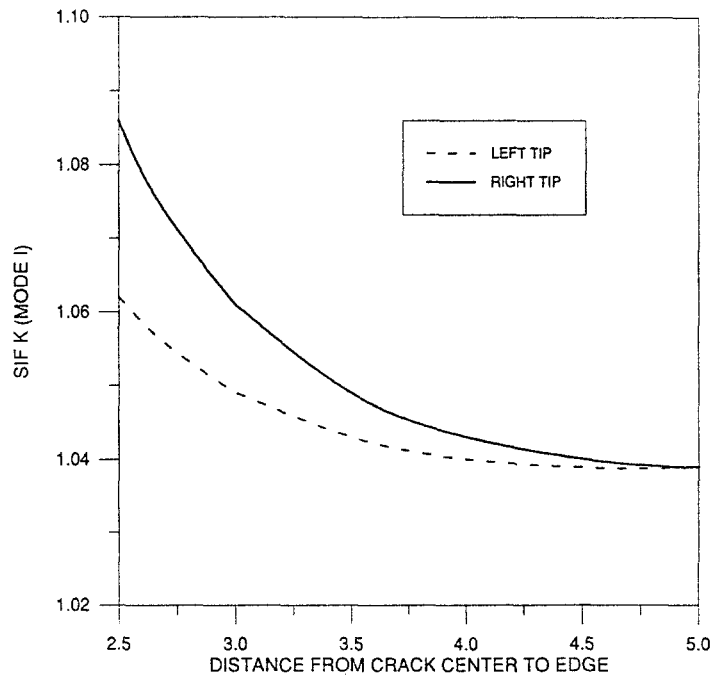


Fig. 8. Variation, with distance to the plate edge, of the normalized stress intensity factors $K_I/(T\sqrt{a})$ at left and right crack tips for the glass/epoxy material. The crack angle $\theta = 0^\circ$ and material angle $\alpha = 0^\circ$.

Table 3. Convergence of mode I stress intensity factors in Glass/Epoxy plate (α = crack orientation)

DOF	$K_I(\alpha = 0^\circ)$	$K_I(\alpha = 45^\circ)$
47	1.082	0.545
71	1.085	0.541
95	1.086	0.540
119	1.086	0.540

For the case of the crack center at a distance of 2.5 times the crack length from the right hand edge, the convergence of the mode I values is presented in Table 3. The material is Glass/Epoxy and two crack orientations, with respect to the material, are considered. It is clear that in both cases the values stabilized after using 95 degrees of freedom.

8. Conclusions

The edge function method has been used to examine a number of issues related to cracks in finite anisotropic plates. Accurate values of stress intensity factors are obtained using a small number of degrees of freedom. Some special test cases have shown close agreement with other published results.

Convergence of the method is influenced by the rate of decay of the line edge functions and crack edge functions away from their respective local axes. The faster the rate of decay the less perturbation induced on other boundaries. The edge functions decay most rapidly and hence do not create a significant disturbance on crack boundaries. This feature explains the more rapid convergence on the crack boundaries as distinct from the straight edge boundaries where the influence of crack edge functions from a nearby crack may be significant. Indeed it is found that several extra orders of line edge functions are required to model the effects on the edge closest to the crack tip in the cases where the crack is moved close to that boundary.

The examples considered above suggest that the effects of the anisotropy are not very significant in determining values of stress intensity factors when the crack is far away from the outer boundaries and the material axes are horizontal. The Graphite/Epoxy material is strongly anisotropic but even in that case there is no major deviation away from the isotropic results. Some effects of the anisotropy are apparent however when the material orientation is varied.

An interesting extension of the present work would be to examine the case of several interacting cracks. This analysis would be analogous to studying the effects of damage accumulation in a composite. Each crack would require its own set of crack functions, which would obviously increase the total number of degrees of freedom required to obtain an accurate solution. However this number would still be much smaller than that for conventional methods. This was shown in an example involving two cracks, which is presented in Dwyer and Amadei [24].

Another aspect of damage progression could be studied by modeling crack propagation. This could be achieved by using the stress intensity factors to determine the direction of propagation and then carrying out an edge function analysis of the new problem with the

crack at a more advanced position. The method is well suited to this type of analysis since only new crack edge functions would be required and the remainder of the model remains the same. This is in contrast to the type of extensive remeshing necessary in a typical finite element analysis. A disadvantage of the current program, however, is the inability to model a curved crack which would constitute a more realistic form of propagation. The model is also limited at present to embedded cracks and an alternative formulation would be required to handle edge cracks.

Acknowledgements

The authors would like to thank Prof. B. Amadei for his encouragement and constructive comments on the paper. The support of the National Science Foundation under grant MS 9215397 and of the Department of Energy under grant DE-FG 03-93-ER61689 is greatly appreciated.

References

1. J.F. Dwyer, Ph.D thesis, University College Cork, Ireland (1986).
2. T.H.H. Pian, P. Tong and C.K. Luk, *3rd Air Force Conference on Matrix Methods in Structural Mechanics* (1971).
3. J.F. Mandell, F.J. McGarry, S.S. Wang and J. Im, *Journal of Composite Materials* 8 (1974) 106–117.
4. R.D. Foschi and D. Barrett, *International Journal for Numerical Methods in Engineering* 10 (1976) 1281–1287.
5. P. Tong, *International Journal for Numerical Methods in Engineering* 11 (1977) 377–403.
6. M.L. Soni and M. Stern, *International Journal of Fracture* 3 (1976) 331–344.
7. S.N. Atluri, A.S. Koyabashi and M. Nakagaki, *ASTM STP* 593 (1975) 86–98.
8. M.D. Snyder and T.A. Cruse, *AFML-TR-73-209* (1973).
9. G. Karami and R.T. Fenner, *International Journal of Fracture* 30 (1986) 13–29.
10. G.E. Blandford, A.R. Ingraffea and J.A. Liggett, *International Journal for Numerical Methods in Engineering* 17 (1981) 387–404.
11. T.A. Cruse and R.B. Wilson, *Nuclear Engineering and Design* 46 (1978) 223–234.
12. D.L. Bowie and C.E. Freese, *International Journal of Fracture* 8 (1972) 49–58.
13. D.L. Bowie and D.M. Neal, *International Journal of Fracture* 6 (1970) 199–206.
14. K.R. Gandhi, *Journal of Strain Analysis* 7 (1972) 157–163.
15. Y.J. Yum and C.S. Hong, *International Journal of Fracture* 47 (1991) 53–67.
16. G.S. Gyekenyesi and A. Mendelson, *Nasa TN D-7119* (1972).
17. P.K. Satapathy and H. Parhi, *International Journal of Engineering Science* 16 (1978) 147–154.
18. K.-L. Chen and S.N. Atluri, *Engineering Fracture Mechanics* 36 (1990) 327–340.
19. C.W. Woo and Y.H. Wang, *International Journal of Fracture* 62 (1993) 203–218.
20. H.C. Chen and J.N. Kudva, *International Journal of Fracture* 63 (1993) 215–228.
21. S.G. Lekhnitskii, *Theory of Elasticity of an Anisotropic Elastic Body*, Holden-Day Inc. (1963).
22. J.J. Grannell and P.M. Quinlan, *Proceedings of the Royal Irish Academy* 80A, 1 (1980) 1–22.
23. J.F. Dwyer and B. Amadei, *Rock Mechanics and Rock Engineering* (accepted for publication).
24. J.F. Dwyer and B. Amadei, *International Journal of Rock Mechanics and Mining Sciences and Geomechanics Abstracts* 32, 2 (1995) 121–133.